2D Kagomé ordering in the 3D frustrated spinel $Li_2Mn_2O_4$

2005 J. Phys.: Condens. Matter 17 6469

(http://iopscience.iop.org/0953-8984/17/41/017)

INSTITUTE OF PHYSICS PUBLISHING JOURNAL OF PHYSICS: CONDENSED MATTER

J. Phys.: Condens. Matter **17** (2005) 6469–6482 doi:10.1088/0953-8984/17/41/017

2D Kagomé ordering in the 3D frustrated spinel $Li_2Mn_2O_4$

C R Wiebe[1,2,4], P L Russo[1], A T Savici[1], Y J Uemura[1], G J MacDougall[2], G M Luke[2], S Kuchta[3] and J E Greedan[3]

[1] Department of Physics, Columbia University, New York, NY 10027, USA
[2] Department of Physics and Astronomy, McMaster University, Hamilton, ON, L8S 4M1, Canada
[3] Department of Chemistry, McMaster University, Hamilton, ON, L8S 4M1, Canada

E-mail: cwiebe@magnet.fsu.edu

Received 18 July 2005, in final form 25 August 2005
Published 30 September 2005
Online at stacks.iop.org/JPhysCM/17/6469

Abstract

Muon spin relaxation (μSR) experiments on the geometrically frustrated spinel oxide, $Li_2Mn_2O_4$, show the development of spin correlations over a range of lengthscales with decreasing temperature. Increased relaxation below ~150 K is consistent with the onset of spin correlations. Below 50 K, spin order, on a lengthscale which is long range for the μSR probe, appears abruptly in temperature, consistent with prior neutron diffraction results. The oscillations in the zero field asymmetry are analysed using a three frequency model. By locating the muon site, this is shown to be consistent with the unexpected 2D $q = \sqrt{3} \times \sqrt{3}$ structure on the Kagomé planes proposed originally from neutron data. Longitudinal field data demonstrate that some spin dynamics persist even at 2 K. Thus, a very complex magnetic ground state, featuring the coexistence of long lengthscale 2D ordering and significant spin dynamics, is proposed. This is unusual considering the 3D topology of the Mn^{3+} spins in this material.

(Some figures in this article are in colour only in the electronic version)

1. Introduction

The phenomenon of geometric frustration is now seeing a surge of interest due to the growing number of unique ground states which arise from networks of spins in triangular motifs [1, 2]. In particular, over the last few years, discoveries such as heavy-fermion behaviour [3], spin-ice ordering [4], and even novel superconductivity [5], have been observed in materials which have magnetic sublattices of corner-shared tetrahedra (such as the spinels and pyrochlores). This has led to increased theoretical interest in these systems, which were originally suggested

[4] Present address: Department of Physics, Florida State University, and the National High Magnetic Field Laboratory, Tallahassee, FL 32310-4005, USA.

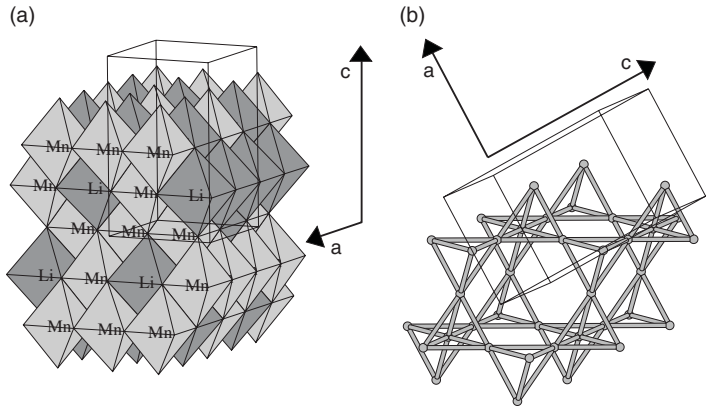

Figure 1. (a) A polyhedral representation of the structure of $Li_2Mn_2O_4$ showing the Li–O and Mn–O octahedra. The Li ions have migrated from the tetrahedral sites in the normal spinel, $LiMn_2O_4$, to the octahedral sites in $Li_2Mn_2O_4$. (b) The Mn magnetic sublattice, shown as a network of corner-shared tetrahedra (which would be identical to the cubic pyrochlore sublattice if not for the tetragonal distortion). This can be described as Kagomé layers which alternate with triangular planar layers in the stacking direction normal to the ⟨111⟩ direction.

by Anderson to be excellent candidates for exotic magnetism, such as the dynamic resonating valence bond state [6]. Although very few examples in the literature exist of this elusive class of materials, new discoveries of the complex magnetism in these systems continue to intrigue the condensed matter community.

One of the more curious discoveries of late lies within the spinel materials $Li_{1+x}Mn_2O_4$. These were once targets for the lithium ion battery community, but they were later discovered to have complicated magnetic properties based upon the frustrated sublattice that they have in common. Complete removal of Li species results in λ-MnO_2, which orders below 32 K into a magnetic unit cell with 256 spins [7]. The next member in the series, $LiMn_2O_4$, exhibits partial Mn^{3+}/Mn^{4+} charge ordering at 280 K followed by a very complex 3D long-range magnetic order below 60 K. Remarkably, the long-range order coexists with short-range, nearest-neighbour lengthscale, order down to the lowest temperature investigated, 1.5 K [8, 20]. But it is the material $Li_2Mn_2O_4$ [9] which has perhaps the most remarkable ground state. This material is synthesized by chemie douce, or soft chemistry insertion of Li ions into $LiMn_2O_4$. The magnetic sublattice, which is populated by Mn^{3+} spins, has a slight tetragonal distortion (due to the Jahn–Teller effect) from the ideal corner-shared tetrahedral network that is seen in the cubic pyrochlores. Nonetheless, this distortion is small, and the sublattice remains, topologically, three dimensional (see figure 1). DC magnetic susceptibility data showed signs of short-range correlations up to $T \sim 400$ K. Neutron diffraction on powder samples revealed broad features indicative of short-range magnetic correlations appearing below 150 K. With decreasing temperature these features took on a pronounced Warren lineshape, a signature of 2D correlations [10]. This is a remarkable result given the 3D topology of the Mn sublattice. The intensity of the Warren reflections increased sharply between 50 and 40 K in an almost first-order fashion. The maximum 2D spin correlation length, obtained by fitting to the Warren function, was ∼90 Å, a relatively large but finite value, which remained unchanged from 40 to 1.6 K. From the positions of the magnetic reflections, the authors suggested that the 2D correlations could be assigned to a $q = \sqrt{3} \times \sqrt{3}$ structure (so called because of the increased area of the unit cell) confined to the Kagomé sheets (see figure 1), but this assignment was based on the observation of only two magnetic reflections [9].

In this paper, muon spin relaxation (μSR) experiments confirm the onset of a long-ranged (on the μSR lengthscale) spin ordering below 50 K, and show evidence for spin correlations setting in below 150 K. Moreover, substantial evidence is provided for the $q = \sqrt{3} \times \sqrt{3}$ magnetic structure on Kagomé layers proposed from the neutron data, and may suggest either a 2D order parameter, or the first-order nature of the transition.

2. Experimental procedure and results

2.1. Sample preparation and characterization

$Li_2Mn_2O_4$ was synthesized according to the method of Wills *et al* by chemie douce, or soft chemistry insertion of Li ions into $LiMn_2O_4$. $LiMn_2O_4$ was prepared by reacting stoichiometric amounts of Li_2CO_3 and Mn_2O_3 in air at 650 °C for 12 h and 800 °C for 24 h, followed by a gradual cooling to room temperature. The product was reground and refired according to the same heating routine and then tested for phase purity by x-ray diffraction using $K\alpha_1$ radiation on a Bruker D8 diffractometer. The Li insertion step was completed in an Ar glove box. Three grams of finely ground $LiMn_2O_4$ were added to 12.5 ml of 16 M *n*-butyl lithium in 40 ml of sodium-dried hexane. This provides a slight excess of *n*-butyl lithium. After gentle heating at 40 °C for 5 days, the final product was filtered and washed well with sodium-dried hexane. The product was tested for phase purity using a Guinier–Hägg camera in a sealed Mylar sample holder.

The magnetic susceptibility was measured in a sealed capsule using a Quantum Design SQUID magnetometer. The experiments were completed in field-cooled (FC) and zero field-cooled (ZFC) sequences and using the reciprocating sample option (RSO) mode on the instrument. μSR experiments were completed by enclosing the sample in a Mylar-sealed sample holder with He exchange gas. All experiments were completed at the M20 beamline at TRIUMF, Vancouver, Canada in a He-flow cryostat which reached temperatures from 2 to 150 K. Zero-field (ZF) and longitudinal field (LF) measurements were made in applied fields of up to 2 kG.

2.2. Muon spin relaxation

Muon spin relaxation, or μSR, has proven to be an invaluable tool of the modern experimental condensed matter physicist [11]. The advantages of this method include the extreme sensitivity to magnetic ordering, the large range of timescales accessible for measuring electronic phenomena, and the ability to conduct experiments on small samples in a variety of external conditions (such as low temperatures, moderate magnetic fields, and under pressure). A considerable advantage over nuclear magnetic resonance experiments is the 100% spin-polarized muon beam (the weak interaction of pion decay ensures that muon decay products have a polarization opposite to their momenta). These beams are oriented at samples with either a zero applied magnetic field (ZF), a field applied in a longitudinal direction with respect to the initial polarized muon spin (LF), or with a field applied in a transverse direction (TF). After rapid thermalization within the sample, the muons stop within the lattice and begin to feel a local magnetic field. The muon decays with an average lifetime of 2.2 μs to products which include positrons that are measured through a series of counters. Since the positron is preferentially emitted in the direction of the muon spin at the time of decay, the angular distribution of positrons can be used to analyse the polarization of the muon as a function of time by capturing many decay events. A detection scheme of forward (F) and backward (B) counters (relative to the sample in the beam) can be used to measure the asymmetry, which

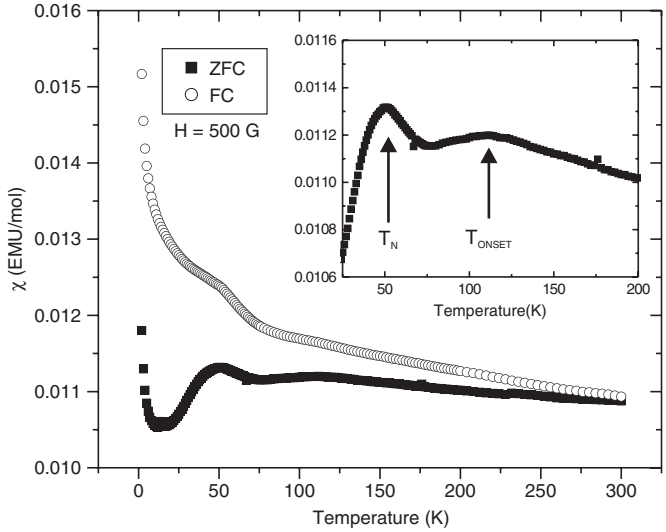

Figure 2. The DC magnetic susceptibility of $Li_2Mn_2O_4$ for an applied field of $H = 500$ G. Zero-field-cooled (ZFC) and field-cooled (FC) data sets are denoted. A broad feature at ∼110 K suggests the onset of magnetic correlations (T_{ONSET}), and a sharper peak at ∼50 K corresponds to the Néel temperature (T_N). The FC/ZFC divergence at higher temperatures is due to magnetic correlations (there is no evidence for impurities through x-ray diffraction measurements).

is simply a normalized difference between the detector count rates (after correcting for solid angle effects).

$$P(t) \sim [F(t) - B(t)]/[F(t) + B(t)]. \tag{1}$$

It is the polarization function $P(t)$ which is measured in μSR experiments.

2.3. Experimental results

DC magnetic susceptibility measurements made in an applied field of 500 G qualitatively reproduced the previous results of Wills and co-workers (see figure 2). There was no Curie–Weiss behaviour detected up to 350 K, and indeed, previous measurements detected no such behaviour up to 800 K [9]. This is a signature of frustrated systems—the Curie–Weiss region is pushed to higher temperatures due to strong antiferromagnetic interactions between the spins. There is also a broad feature at $T \sim 110$ K which makes it difficult to perform a Curie–Weiss analysis. This peak is interpreted as a signature of short-ranged magnetic ordering of the Mn^{3+} spins. A cusp in the susceptibility occurs just below 50 K, indicative of the onset of the relatively long-range 2D order found in the neutron data. The divergence of the FC/ZFC data at high temperatures could be due to a small impurity, or the presence of magnetic correlations. The lack of impurity lines in the x-ray diffraction data suggests the latter explanation over the former.

μSR measurements on powder samples of $Li_2Mn_2O_4$ in zero-field (ZF) identified a two-component lineshape which became prominent below 150 K. This data was fitted to a Kubo–Toyabe function, to account for relaxation processes from nuclear dipoles, and an exponential function, to account for relaxation of magnetic origin. At high temperatures, the nuclear dipole contribution is dominant, but at low temperatures the electronic component begins to grow as the fluctuating spins slow down and enter the μSR time window.

$$P(t) = A(fG_{KT}e^{-\lambda_{slow}t} + (1 - f)e^{-\lambda_{fast}t}) \tag{2}$$

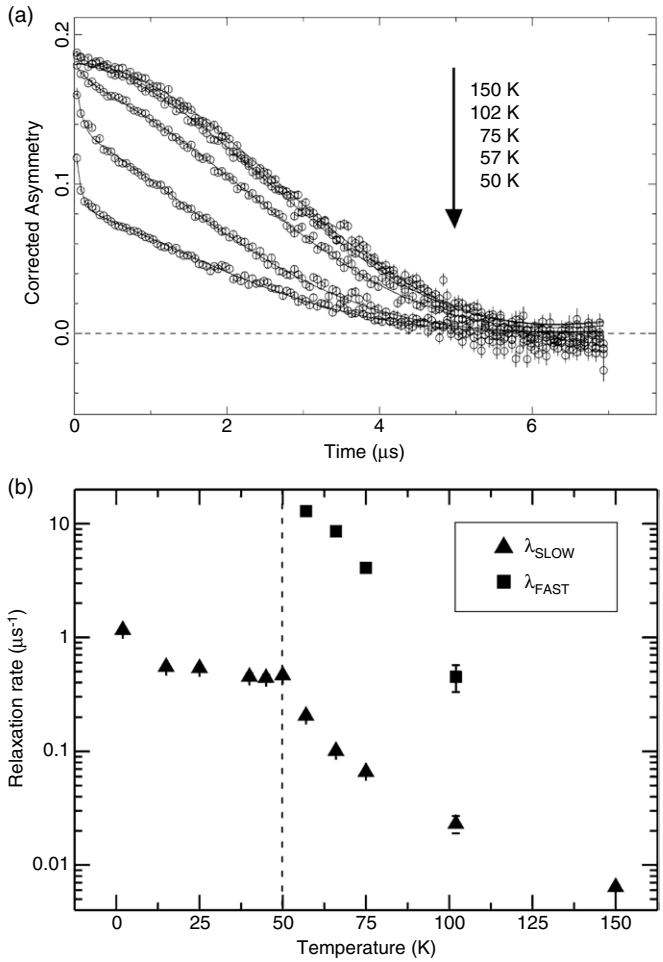

Figure 3. (a) ZF-μSR spectra at 50 K and above with fits described in the text. (b) Relaxation rate of the two components as a function of temperature. Below 50 K, a different fitting function is used for the data.

where $P(t)$ is the muon polarization function, A is the asymmetry, f is the nuclear dipolar fraction of the signal, G_{KT} is the Kubo–Toyabe lineshape, and λ_{slow} and λ_{fast} are the relaxation rates (see figure 3). The former rate is slower than the latter, which accounts for the quasi-static ordering seen above 50 K as a decrease in polarization at early times. The fraction, f, represents the fraction of the slow Kubo–Toyabe signal of the total signal. At high temperatures (i.e. 150 K), this is 1. As one cools down (see figure 5(a)), this fraction decreases as the fast exponential component grows in size. This shows that a separate population of spins starts to slow down and grow in size below 150 K, which correlates nicely with the broad feature in the DC susceptibility at 110 K. At 57 K, this population represents about 25% of the total asymmetry. Below 50 K, about a third of the asymmetry is oscillating (corresponding to about 50% of the spins ordered).

The Kubo–Toyabe lineshape is, explicitly,

$$G_{KT} = \tfrac{1}{3} + \tfrac{2}{3}(1 - \Delta^2 t^2)e^{-\Delta^2 t^2/2} \tag{3}$$

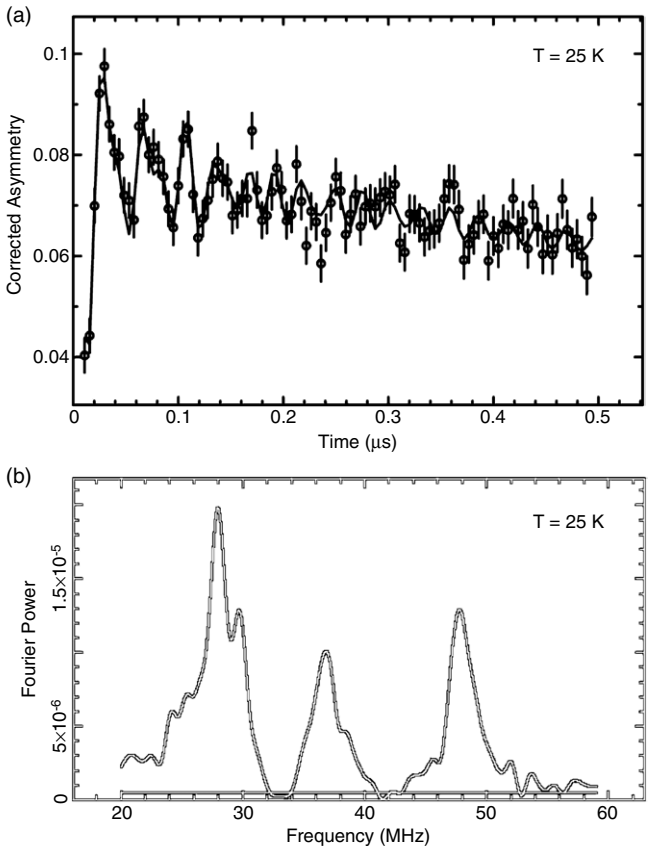

Figure 4. (a) Early time ZF-μSR spectra at $T = 25$ K. The fit is to a three-frequency model. (b) The Fourier transform of these data, showing three distinguishable components.

where Δ^2 is the second moment of the field distribution of nuclear dipolar origin. A rise in the relaxation rate to a maximum at 50 K is typical of the dynamics associated with magnetic transitions to long-range ordered ground states. The physical origin of this is the longer correlation times near a phase transition (known as critical slowing down). The lack of a sharp maximum at 50 K could be due to either the coarseness of the temperature steps near T_N, or the abrupt nature of the transition. The appearance of a second component at temperatures much larger than 50 K, however, is unusual and its origin is due to the gradual slowing down of spins over decades in temperature (another common feature of magnetically frustrated systems). A likely cause of this is the formation of short-ranged spin correlations, as suggested by previous neutron work. It is also unusual that the relaxation persists to temperatures below 50 K. This is evidence for fluctuating spins coexisting with ordered spins as $T \to 0$ K. Further signatures of the dynamic nature of this ground state are seen in the longitudinal field measurements (LF), which show that even strong fields do not completely decouple the signal.

ZF-μSR spectra taken below 50 K show an oscillating component from muon precession in a local internal magnetic field. Fourier transforms revealed three well-defined frequencies, which were used to fit the data below 50 K in the regime $0\,\mathrm{s} < t < 2\,\mu\mathrm{s}$ (see figure 4). For longer timescales, the data was fitted to a Kubo–Toyabe lineshape multiplied by an exponential.

$$P(t) = A_0 G_{KT} e^{-\lambda_{slow} t} + A_1 \cos(\omega_1 t) e^{-\lambda_1 t} + A_2 \cos(\omega_2 t) e^{-\lambda_2 t} + A_3 \cos(\omega_3 t) e^{-\lambda_3 t}. \quad (4)$$

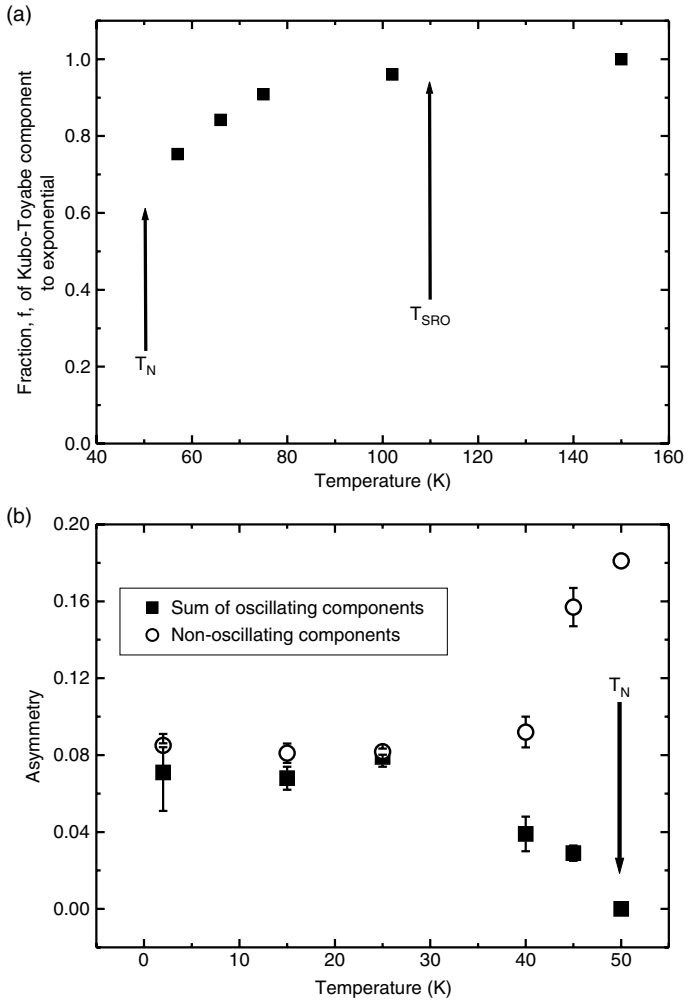

Figure 5. (a) The temperature dependence of the Kubo–Toyabe signal to the exponential signal above 50 K. (b) The temperature dependence of the three oscillating components (summed together) and the non-oscillating Kubo–Toyabe function (multiplied by an exponential).

In this equation, A_i, λ_i, and ν_i are the asymmetries, relaxation rates, and frequencies of the three oscillating components, respectively, and A_0 is the asymmetry of the Kubo–Toyabe component. A common phase, ϕ, was used for the three components for the initial fitting process. Since this was within error of zero, the phase was set to zero for the final fits.

The asymmetries of the oscillating and non-oscillating components are noted in figure 5. The drop in asymmetry of the ordered signal at 50 K coincides with a rise of the Kubo–Toyabe/exponential signal.

The asymmetry of the oscillating components was found to be only about a third of the expected total asymmetry, suggesting that only a portion of the spins are ordered at 2 K. The remainder of the spins are either still fluctuating or in short-ranged ordered spin clusters. The three-frequency fit represents the data well; however, the corresponding temperature dependence of all three components is uncharacteristic of 3D ordering. All three show a very rapid increase to saturation below 50 K.

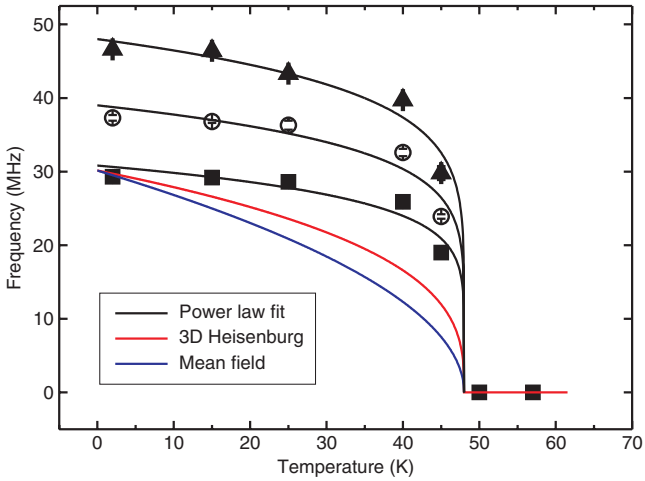

Figure 6. The temperature dependence of the three fitted frequencies. A power-law exponential has been fitted to the lowest frequency with $\beta = 0.14(3)$. The two higher frequencies show the same fit for the lower frequency with a normalization factor. For comparison, the expected power laws for 3D Heisenburg and mean field theory have been shown.

The low-frequency component of the data has been fitted to the phenomenological form

$$\nu = \nu_0(1 - T/T_N)^{\beta} \tag{5}$$

where β is the critical exponent. Although a rigorous examination of the power law would require more points around T_N, it is clear that the transition is not mean-field like ($\beta = 0.5$), or 3D Heisenburg ($\beta = 0.33$), as shown in figure 6. The fit, to free parameters for β, ν_0, and T_N for the lowest-frequency component, is $\beta = 0.14(3)$, which is more consistent with the 2D Ising critical exponent of $\beta = 0.125$, and a transition temperature of 48 ± 2 K. The rapid increase of the precession frequency is also characteristic of a first-order-like transition, which is echoed in the spin–spin correlation lengths extracted from neutron scattering measurements.

The relaxation rate of the $1/T_1$ tail (λ_{slow}) is approximately a constant below T_N. This is strong evidence that there are coexisting regions of ordered and disordered spins. Since the behaviour of the disordered spins (from the $1/T_1$ tail) changes abruptly below T_N, these spins must be involved with the transition (it is unlikely that there is bulk phase separation).

LF-μSR spectra show that most of the signal is decoupled with the application of applied magnetic fields. This indicates that there is a large population of static spins. However, there is a small fraction of spins (about 10% of the total volume fraction) which do not decouple, even down to 2 K and in strong fields (see figure 7 at $T = 2$ and 66 K). This suggests the coexistence of magnetic order and regions of persistently fluctuating moments.

3. Discussion

Our μSR results present strong evidence for the model proposed by [9], i.e. a $q = \sqrt{3} \times \sqrt{3}$ ordering for the Mn spins in the Kagomé layers. Below 50 K, there appears to be a population of spins (roughly 50%) which lie in an ordered state with respect to the muon timescale. In order to shed some light on the nature of this ordering, one must first attempt to identify the muon site. Given that there are three separate frequencies in the data, the first place to start is to assume that the muon is experiencing three distinct internal fields from either the

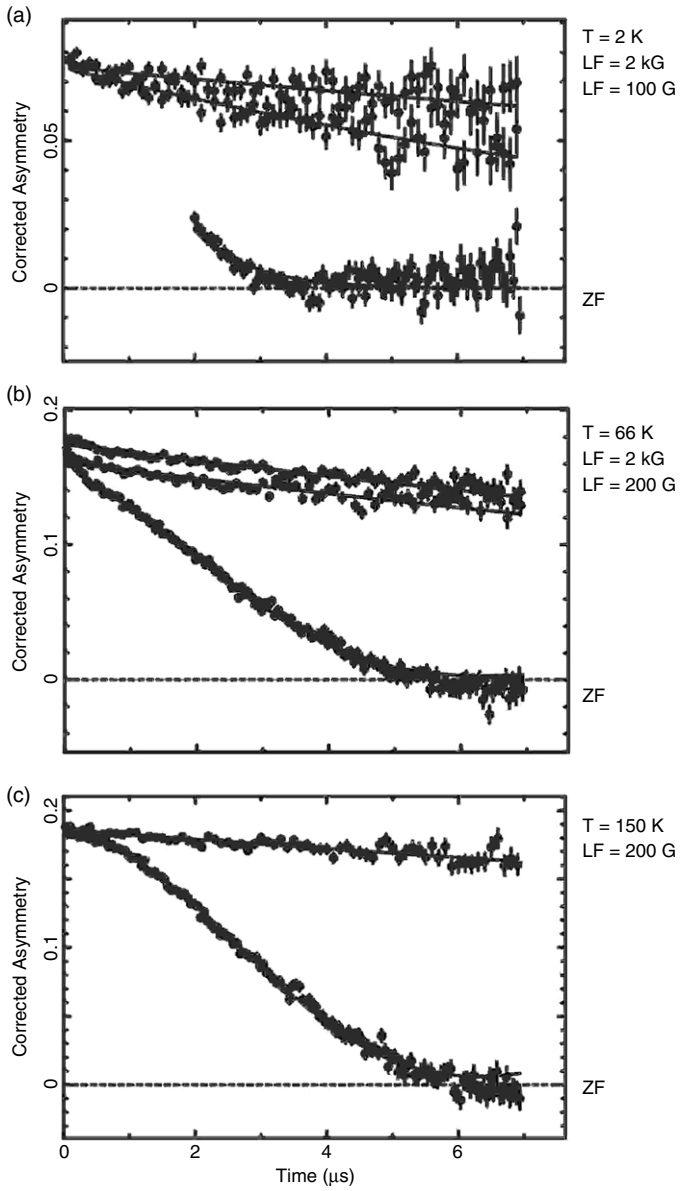

Figure 7. ZF and LF μSR data at (a) $T = 2$ K, (b) $T = 66$ K, (c) $T = 150$ K. The data at 2 K in ZF have been omitted in the early time signal where oscillations are observed.

magnetic structure or different muon sites or both. It is therefore important to locate the muon sites within $Li_2Mn_2O_4$. The most probable site is one which is equidistant from the oxygen positions. There are three obvious choices for this: at the interstitial sites $(3/8, 3/8, 3/8)$, $(1/4, 1/4, 1/4)$, or $(0, 0.75, 0.125)$. Detailed calculations of the field experienced by the muon at each site were made by using the equation

$$\Delta^2 = \frac{4}{9}\gamma_\mu^2 \sum \overline{\mu_i^2} \frac{1}{r_i^6} \tag{6}$$

Table 1. Possible muon sites with the calculated relaxation rate. The (0, 0.75, 0.125) position has a value which is closest to the fits derived from the muon data ($\Delta = 0.275\ \mu s^{-1}$).

Muon site	Δ (μs^{-1})	Comment
(1/4, 1/4, 3/4)	0.132	Occupied by Li
(3/8, 3/8, 3/8)	0.418	Interstitial
(0, 0.75, 0.125)	0.308	Interstitial

in which γ_μ is the muon gyromagnetic ratio (135.5 MHz T^{-1}) and μ_i is the dipolar moment at site i at a distance r_i from the muon site. This is the relaxation rate Δ (due to random nuclear dipolar fields) which is extracted from the Kubo–Toyabe fits to the high-temperature data (150 K). Sums were made over several unit cells in length in the three crystallographic directions. The theoretical values for the relaxation rates at the three sites of interest are listed in table 1.

In the material $LiMn_2O_4$, the most probable site is in the interstitial position (1/4, 1/4, 3/4), where the muon has some mobility within the lithium-depleted structure acting like a Li^+ ion. This has been verified by detailed μSR experiments and calculations on $LiMn_2O_4$ [12]. However, in $Li_2Mn_2O_4$, all of these sites are filled by intercalated lithium atoms. The calculated relaxation rate of 0.132 μs^{-1} does not agree with the value found from the Kubo–Toyabe fits of 0.275 μs^{-1}, suggesting that another muon site is a better choice.

The site (3/8, 3/8, 3/8) is in an electrostatically favourable environment, surrounded by six oxygens in an octahedral framework at distances of 1.5–2.6 Å. This position was found to be the muon site for the spinel LiV_2O_4 in a recent μSR study [13]. However, the theoretical value for the relaxation rate from this field distribution is 0.418 μs^{-1}, which does not agree with the value obtained from our data.

The best agreement with our high-temperature Kubo–Toyabe fits to the relaxation rate of 0.275(1) μs^{-1} is at the (0, 0.75, 0.125) position. It is perhaps not surprising that this is the most probable muon stopping site for $Li_2Mn_2O_4$. This is a tetrahedral site where Li resides in $LiMn_2O_4$, but it is not occupied in $Li_2Mn_2O_4$ according to previous diffraction studies (all of the lithium atoms are at the octahedrally coordinated 8c site (0, 0, 0)). This is, therefore, a favourable position for the muon, which will act like a Li^+ cation surrounded by a four-fold oxygen cage at distances of 1.92 Å. It is also surrounded by four equidistant Li^+ cations at distances of 1.82 Å.

Given this result, one can now shed some light on the muon precession frequencies observed at the ordering transition. Wills and co-workers suggested that a $q = \sqrt{3} \times \sqrt{3}$ Kagomé ordering is present within the pyrochlore Mn magnetic sublattice. This leaves two separate magnetic species—the ordered spins which lie within the Kagomé layers and the disordered spins in the adjacent triangular plane layers. Figure 8 shows this explicitly, with the muon stopping sites indicated. These are located slightly above and below the Kagomé planes, at positions roughly in the middle of each Kagomé plaquette. Three different muon precession frequencies are seen for our data, at roughly 46, 37, and 30 MHz, corresponding to three different internal fields seen by the muon. To see how this could arise in the $q = \sqrt{3} \times \sqrt{3}$ spin structure, consider figure 9. The two possible spin structures are plotted with respect to the muon stopping sites, which lie at positions just above and below the planes as indicated. For the $q = 0$ structure, the muons all experience virtually the same spin environment within the magnetic unit cell. In the upper limit, the muon can feel two frequencies within the unit cell (one for each stopping site). However, there are six different internal fields experienced by muons within the $q = \sqrt{3} \times \sqrt{3}$ magnetic unit cell. Detailed calculations of the internal fields using dipolar interactions between the moments and the muon sites reveal that there are indeed

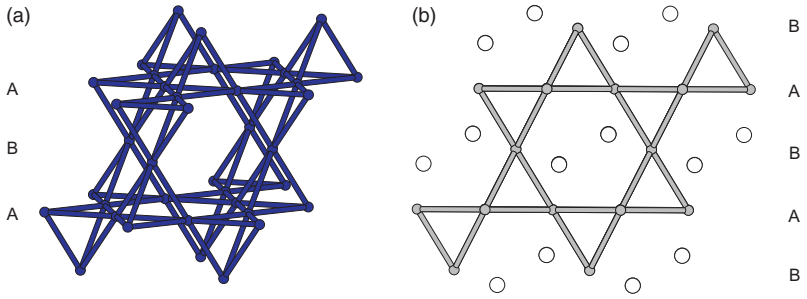

Figure 8. (a) The Kagomé magnetic sublattice within the spinel structure. A and B indicate the alternating Kagomé and triangular planar layer sites, respectively. (b) The muon stopping sites with respect to the Kagomé (A) and interconnecting layers (B).

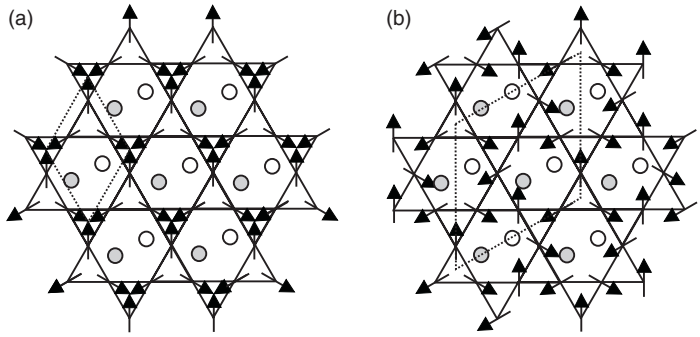

Figure 9. (a) The $q = 0$ Kagomé structure and (b) the $q = \sqrt{3} \times \sqrt{3}$ structure. The muon sites in $Li_2Mn_2O_4$ are indicated on the figures as circles, slightly above (grey) and below (white) the Kagomé planes. The magnetic sublattices in 2D are marked by dashed lines. There are two muon sites for the $q = 0$ structure, but six sites for the $q = \sqrt{3} \times \sqrt{3}$ structure.

Table 2. Experimental frequency ratios for precession components at 2 K. The ratios of these frequencies are compared to the calculated values for the muon site in the $\sqrt{3} \times \sqrt{3}$ structure.

Frequency (MHz)	Ratio (exp.)	Ratio (calc.)
29.3 ± 0.4	—	—
37.3 ± 0.4	1.27 ± 0.04	1.34
46.4 ± 0.4	1.58 ± 0.04	1.46

three frequencies experienced by the muons—four sites which are nearly degenerate with a low frequency, and the remaining two sites with higher frequencies. Table 2 shows these results explicitly, with excellent agreement shown with the ratios of the three frequencies observed in our data. This also is in qualitative agreement with the distribution of components in the Fourier transform, which reveals a broad set of frequencies centred about 30 MHz (from the four nearly degenerate fields), and two smaller components at 37 and 46 MHz (from the other two fields observed). In conclusion, one can say with some confidence that the $q = \sqrt{3} \times \sqrt{3}$ structure is consistent with the distribution of frequencies observed in our data, given our choice of muon site. The $q = 0$ structure cannot give rise to three unique muon frequencies.

With this excellent agreement of the internal field at the muon sites with respect to the ratios of the frequencies observed, one can now estimate the size of the average static moment at the Mn^{3+} site. This is done by evaluating the size of the field at these points by dividing

the precession frequency by the muon gyromagnetic ratio ($\gamma_\mu = 135.5$ MHz T^{-1}), and then comparing this to our calculations of the frequency distribution. The resultant average static moment of 1.5(1) μ_B per atom falls short of the expected value for Mn^{3+} moments of 4.0 μ_B. Reduced moments are common in magnetically frustrated systems [2]. Another possible origin of the small moment is that there are some disordered spins within the ordered Kagomé layers, leading to a lower average static moment.

In subsequent LF-μSR experiments, we observed that applied fields do not completely decouple the signal (see figure 6), which suggests that the dynamics are not quenched easily. The rise of the relaxation rate to a constant value below 50 K is consistent with a dynamic ground state as well. Other frustrated systems, such as $Tb_2Ti_2O_7$, show this behaviour, which has been interpreted as a ground state stabilized by quantum fluctuations [14]. The asymptotic relaxation rate, $\sim 1\ \mu s^{-1}$, is of the same order of magnitude. This distinguishes the behaviour of this system from that associated with glassy spin freezing, such as is seen in $Y_2Mo_2O_7$, which has a prominent cusp in the relaxation rate and a low-temperature value which is about 250 times smaller than $Li_2Mn_2O_4$ [15]. Highly correlated dynamics typical of frustrated materials, such as spin-liquid behaviour [16], would give rise to purely exponential relaxation, or 'undecouplable' Gaussian features in zero-field μSR [17]. $Li_2Mn_2O_4$ is qualitatively different from either a pure spin glass or a pure spin liquid, with the coexistence of ordered and fluctuating spins.

With respect to other spinel oxides, $Li_2Mn_2O_4$ has common features with materials such as $ZnFe_2O_4$. The low-temperature ground state of $ZnFe_2O_4$ is an ordered antiferromagnet with a $k = (0, 0, 0)$ wavevector at 10 K [19]. However, it has been known for some time that a short-range ordered state exists at temperatures much higher than T_N—as high as 100 K. Broad peaks appear in elastic neutron scattering experiments which persist to low temperatures. In addition, the μSR data on this material show a two-component lineshape below 100 K in accordance with the slowing down of spins in a short-range ordered state. With neutron and μSR studies combined, the consensus is that at $T_N = 10$ K, only about 30% of the volume fraction is long-range ordered. The remaining fraction are in 'superantiferromagnetic' clusters of short-range ordered spins with sizes of about 30 Å (incidentally, this is in good agreement with the spin–spin correlation length in the $Li_2Mn_2O_4$ neutron scattering data of about 20 Å at 100 K [9]). The similarities between these two materials are considerable, both with short-range ordered states at high temperatures, followed by a transition to a coexisting long-range ordered state at low temperatures. The μSR data on $ZnFe_2O_4$ suggests that there is some competition between these two states below T_N, with the volume fraction of the LRO clusters becoming larger at the expense of the SRO clusters. This has not been observed in $Li_2Mn_2O_4$. Larger fields are also needed to decouple the LF-μSR data in $ZnFe_2O_4$, which suggests that significant dynamics play a role at low temperatures. The ground state is inhomogeneous in both cases, but notable differences exist between these two materials.

A closer relative to $Li_2Mn_2O_4$ is the single-lithiated spinel $LiMn_2O_4$. As mentioned above, this material orders into an LRO state at 60 K. The magnetic unit cell is enormously complicated, with a $k = (1/2, 1/2, 1/4)$ structure and 1152 spins within [8]. A detailed magnetic structure is at this time unavailable. However, it is known that there is an SRO state which exists to high temperatures. Recently, spin polarized neutron scattering measurements revealed that above $T_N = 65$ K the observable magnetic cross section is entirely due to SRO spins on a lengthscale of $\sim$3.5 Å (second Mn neighbours) [20]. As the temperature is reduced below T_N, the fraction of the total magnetic cross section associated with LRO increases, reaching a maximum value of only 50% at 1.5 K. Inelastic scattering shows that even at 1.5 K, $\sim$20% of the spins are still fluctuating. $LiMn_2O_4$ thus shows a complex magnetic ground state with coexisting 3D LRO, SRO, and fluctuating spins. This is similar to the situation found

for $Li_2Mn_2O_4$ but the details are different as there is no true LRO in this material but only 2D SRO of significant, but finite, extent at the lowest temperatures.

In broader terms of comparison, $Li_2Mn_2O_4$ is very distinct from other frustrated sublattices. $Gd_2Ti_2O_7$ has been suggested to be an example of a system which has a Kagomé ordering on a pyrochlore lattice [21]. The mechanism is very different in this case, with dipolar interactions influencing the low-temperature physics of the Gd moment ordering. Furthermore, it has been recently shown that even though a partially ordered structure develops at 1.1 K, the remainder of the spins order at 0.7 K in a multi-k structure [22–24]. The real canonical examples of the 2D Kagomé lattice, however, are not the pyrochlores but the jarosites. For years, $SrCr_xGa_{12-x}O_{19}$ (SCGO) was considered to be an example of the unusual physics which develops in Kagomé systems, being a material which has exhibited spin-glass to spin-liquid characteristics depending on the Cr-site coverage and sample quality [17, 18]. However, this material, being of the magnetoplumbite structure, is better described as an array of bilayer Kagomé units rather than the pure structure. The jarosites, of general formula $AB_3(SO_4)_2(OH)_6$, with B being the magnetic species, represent the best physical realization of the Kagomé lattice [25, 26]. Although disorder within these layers is common, most of these materials have a high site coverage that is still within the percolation limit. A large portion of them form LRO ground states as well, in either the $q = 0$ or $q = \sqrt{3} \times \sqrt{3}$ structures [27]. The latter structure has been shown to be more stable than the former due to quantum effects which choose this state from the multitude of classically degenerate states [28]. However, if one includes next-nearest-neighbour interactions, the situation becomes more complicated. For second-neighbour (J_2) and third-neighbour interactions (J_3), the $q = 0$ state is preferred for $J_2 > J_3$ and the $q = \sqrt{3} \times \sqrt{3}$ for $J_2 < J_3$ [29]. The situation becomes even more elaborate if interplane interactions are considered as well [30]. More detailed studies are needed to clarify the nature of the spin interactions in $Li_2Mn_2O_4$, such as been done for the jarosite $KCr_3OD_6(SO_4)_2$ with inelastic neutron scattering experiments [31].

It is unclear why a 3D system such as $Li_2Mn_2O_4$ would order with small regions of correlated 2D spins. Although these spin clusters have been observed in other spinels, as mentioned above, there is as yet no explanation for why this would occur. The most intriguing work of late is on the spinel $ZnCr_2O_4$, in which the authors, through neutron scattering experiments, demonstrate that hexagonal, 2D spin clusters play an important role in the low-temperature spin dynamics [32]. These hexagonal 'protectorates' form independently of one another, and their excitations are the origin for the local zero-energy modes in the pyrochlore lattice. These spin clusters were noted before in μSR measurements as regions of long-range order (on the muon lengthscale) coexisting with strong spin fluctuations [33]. It is suggested from the neutron work that the formation of spin clusters might be a central theme of self-organization in frustrated materials, which in many cases cannot have conventional Néel ground states. Future work to measure the inelastic spectra of $Li_2Mn_2O_4$ would be essential in elucidating the physics of these many-body systems.

Acknowledgments

CRW would like to acknowledge support from NSERC in the form of a Post-doctoral fellowship. The authors are grateful for the financial support of NSERC and CIAR. The authors are also grateful for the technical support of Bassam Hitti and Don Arseneau at TRIUMF. JEG and GML thank NSERC for support of this work through Discovery Grants. Work at Columbia is supported by NSF-DMR-0102752 and 0502706.

References

[1] Greedan J E 2001 *Chem. Mater.* **11** 37
[2] Ramirez A P 1994 *Annu. Rev. Mater. Sci.* **24** 453
[3] Kondo S *et al* 1997 *Phys. Rev. Lett.* **78** 3729
[4] Bramwell S T and Gingras M J P 2001 *Science* **294** 1495
[5] Hanawa M, Muraoka Y, Tayama T, Sakakibara T, Yamaura J and Hiroi Z 2001 *Phys. Rev. Lett.* **87** 187001
[6] Anderson P W 1956 *Phys. Rev.* **102** 1008
[7] Greedan J E, Raju N P, Wills A S, Morin C and Shaw S M 1998 *Chem. Mater.* **10** 3058
[8] Wills A S, Raju N P and Greedan J E 1999 *Chem. Mater.* **11** 1510
[9] Wills A S, Raju N P, Moran C and Greedan J E 1999 *Chem. Mater.* **11** 1936
[10] Warren B E 1941 *Phys. Rev.* **59** 693
[11] For a review of the μSR technique, see Blundell S J 1999 *Contemp. Phys.* **40** 175
For a general review of μSR experiments on geometrically frustrated materials, see Dalmas de Réotier P, Gubbens P C M and Yaouanc A 2004 *J. Phys.: Condens. Matter* **16** L54687 or the recent conference proceedings on highly frustrated magnetism 2003 in
Dalmas de Rèotier P, Gubbens P C M and Yaouanc A 2003 *J. Phys.: Condens. Matter* **16** (11)
[12] Ariza M J, Jones D J, Roziere J, Lord J S and Ravot D 2003 *J. Phys. Chem.* B **107** 6003
[13] Koda A, Kadono R, Higetomo W, Ohishi K, Ueda H, Urano C, Kondo S, Nohara M and Takagi H 2004 *Phys. Rev.* B **69** 012402
[14] Gardner J S *et al* 1999 *Phys. Rev. Lett.* **82** 1012
[15] Dunsiger S R *et al* 1996 *Phys. Rev.* B **54** 9019
[16] Rovers M T, Kyriakou P P, Dabkowska H A, Luke G M, Larkin M I and Savici A T 2002 *Phys. Rev.* B **66** 174434
[17] Uemura Y J *et al* 1994 *Phys. Rev. Lett.* **73** 3306
[18] Ramirez A P, Espinosa E S and Cooper A S 1992 *Phys. Rev. Lett.* **45** 2505
[19] Schiessl W *et al* 1996 *Phys. Rev.* B **53** 9143
[20] Greedan J E, Wiebe C R, Wills A S and Stewart J R 2002 *Phys. Rev.* B **65** 184424
[21] Champion J D M, Wills A S, Fennell T, Bramwell S T, Gardner J S and Green M A 2001 *Phys. Rev.* B **64** 140407
[22] Stewart J R, Ehlers G, Wills A S, Bramwell S T and Gardner J S 2004 *J. Phys.: Condens. Matter* **16** L321
[23] Bonville P, Hodges J A, Ocio M, Sanchez J P, Vulliet P, Sosin S and Braithwaite D 2003 *J. Phys.: Condens. Matter* **15** 7777
[24] Yaouanc A, Dalmas de Réotier P, Glazkov V, Marin C, Bonville P, Hodges J A, Gubbens P C M, Sakarya S and Baines C 2005 *Phys. Rev. Lett.* **95** 047203
[25] Townsend M G, Longworth G and Roudant E 1986 *Phys. Rev.* B **33** 4919
[26] Wills A S and Harrison A 1996 *J. Chem. Soc. Faraday Trans.* **92** 2161
[27] Keren A, Kojima K, Le L P, Luke G M, Wu W D, Uemura Y J, Takano M, Dabkowska H and Gingras M J P 1996 *Phys. Rev.* B **53** 6451
[28] Sachdev S 1992 *Phys. Rev.* B **45** 12377
[29] Harris A B, Kallin C and Berlinsky A J 1992 *Phys. Rev.* B **45** 2899
[30] Wills A S 2001 *Phys. Rev.* B **63** 064430
[31] Lee S-H, Broholm C, Collins M F, Heller L, Ramirez A P, Kloc Ch, Bucher E, Erwin R W and Lacevic N 1997 *Phys. Rev.* B **56** 8091
[32] Lee S-H, Broholm C, Ratcliff W, Gasparovic G, Huang Q, Kim T H and Cheong S W 2002 *Nature* **418** 856
[33] Marshall I M, Blundell S J, Pratt F L, Husman A, Steer C A, Coldea A I, Hayes W and Ward R C C 2002 *J. Phys.: Condens. Matter* **14** L157